fractal and fractional

MDPI

Article

Dynamic Analysis and Audio Encryption Application in IoT of a Multi-Scroll Fractional-Order Memristive Hopfield Neural Network

Fei Yu [1,*], Qiulin Yu [1], Huifeng Chen [1], Xinxin Kong [1], Abdulmajeed Abdullah Mohammed Mokbel [1], Shuo Cai [1] and Sichun Du [2]

[1] School of Computer and Communication Engineering, Changsha University of Science and Technology, Changsha 410114, China; csust_yql@163.com (Q.Y.); chf_csust@163.com (H.C.); kxx_csust@163.com (X.K.); qubati01@gmail.com (A.A.M.M.); caishuo@csust.edu.cn (S.C.)

[2] College of Computer Science and Electronic Engineering, Hunan University, Changsha 410082, China; jt_dsc@hnu.edu.cn

* Correspondence: yufeiyfyf@csust.edu.cn

Abstract: Fractional-order chaotic systems are widely used in the field of encryption because of its initial value sensitivity and historical memory. In this paper, the fractional-order definition of Caputo is introduced based on a nonideal flux-controlled memristive Hopfield neural network model, when changing the parameters of the fractional-order memristive Hopfield neural network (FMHNN) can generate a different amount of multi-scroll attractors. Some dynamical behaviors are investigated by numerical simulation, especially analyzed coexistence and bifurcation under different orders and different coupling strengths. The results show that the chaotic system of FMHNN has abundant dynamic behaviors. In addition, a chaotic audio encryption scheme under a Message Queueing Telemetry Transport (MQTT) protocol is proposed and implemented by Raspberry Pi; the audio encryption system based on FMHNN has a broad future in intelligent home and other IoT applications.

Keywords: fractional-order; memristive hopfield neural network (MHNN); audio encryption; MQTT for IoT; Raspberry Pi

check for updates

Citation: Yu, F.; Yu, Q.; Chen, H.; Kong, X.; Mokbel, A.A.M.; Cai, S.; Du, S. Dynamic Analysis and Audio Encryption Application in IoT of a Multi-Scroll Fractional-Order Memristive Hopfield Neural Network. *Fractal Fract.* **2022**, *6*, 370. https://doi.org/10.3390/fractalfract6070370

Academic Editors: Yangquan Chen, Ivanka Stamova, Song Zheng and Emad E. Mahmoud

Received: 5 April 2022
Accepted: 21 June 2022
Published: 30 June 2022

Publisher's Note: MDPI stays neutral with regard to jurisdictional claims in published maps and institutional affiliations.

Copyright: © 2022 by the authors. Licensee MDPI, Basel, Switzerland. This article is an open access article distributed under the terms and conditions of the Creative Commons Attribution (CC BY) license (https://creativecommons.org/licenses/by/4.0/).

1. Introduction

Artificial neural network (ANN) is a theoretical model modeled after a biological nervous system, which is composed of neurons and synapses. Neurons have complex nonlinear characteristics and are the basic unit of information processing in biological nervous systems. They can usually realize the basic functions of neurons by feeling stimulus and conducting excitement [1–4]. Neural network (NN) is widely used in image classification, fault diagnosis, deep learning and other fields [5–10]. Neurobiological studies have found that chaos exists in the human brain. Therefore, chaos theory is introduced into ANN to better simulate the neural network structure of the brain. In recent years, the research of chaotic neural network (CNN) has become a hot topic, mainly to establish a variety of neural network models containing chaotic dynamical behaviors [11–16], so as to study the complex chaotic phenomena of the human brain and apply them to intelligent information processing. Due to the introduction of chaotic dynamics, CNN has more dynamic characteristics. The complex dynamic characteristics of CNN make it widely used in information processing, algorithm optimization, image encryption and random number generators [17–21], etc.

Memristor is an electronic component that represents the internal relationship between charge and magnetic flux. Due to its nanoscale, nonlinear and memory characteristics, memristor has a wide application prospect in nonlinear circuits [22–26], chaotic systems [27–32],

memory storage [33–35], neural networks [36–42] and other fields. Further studies show that memristors can simulate synapses in the brain. Because of this memory property of memristors, memristors can be used to replace resistors in traditional neural networks to construct memristive neural networks (MNNs). In recent years, the dynamic behavior of MNNs has been studied extensively [36–40]. A simple local active memristor was proposed in [42] and its state equation was only composed of linear terms. Then, based on the proposed local active memristor, a neural model composed of two 2D HR neurons was established. Based on the 2D discrete Rulkov model, Xu et al. proposed a continuous non autonomous memristive Rulkov model. The current generated by the flux controlled memristor simulated the electromagnetic induction current, and a sinusoidal current was injected into the external stimulation, and then the effects of electromagnetic induction and external stimulation were discussed [43]. In order to study the electromagnetic induction flow in interconnected neurons of Hopfield neural network (HNN), Chen et al. proposed a unified memristive HNN model using hyperbolic-type memristors to link neurons. The authors explored the effect of electromagnetic induction on the memristive HNN with three neurons and discussed three cases [44].

The fractional-order differential system has good historical memory, which is similar to the associative memory of the neural network model [29,45]. The combination of the memristor and fractional-order differential system may improve the memory performance of the system. Researchers began to explore the fractional-order neural network, and carried out extensive research on its dynamic behavior and application [46–49]. Ma et al. studied a fractional-order Hopfield neural network (FHNN) with complex function nonlinear terms based on the Adomian decomposition method, and observed the complex phenomenon of coexistence of attractors in this fractional system [47]. In recent years, fractional-order memristive neural networks (FMNN) have also been studied. Fan et al. proposed a simplified FMNN, which is a switching system with an irregular switching law and consists of eight subsystems [48]. Yu et al. proposed a new 6D fractional-order memristive Hopfield neural network (6D-FMHNN) and investigated the bifurcation and coexistence attractor properties of the 6D-FMHNN [49].

We introduce Caputo fractional-order definition and the Adomian decomposition method to study a nonideal flux-controlled memristor on HNN model. In the extended FMHNN, we found that different dynamical behaviors can be generated by controlling different orders; coexistence and multi-scroll attractors can also be generated by changing system parameters such as synaptic coupling strength. In addition, we use the FMHNN to implement a smart home scenario audio encryption system under an MQTT protocol, and through an embedded device, Raspberry Pi implements a prototype of this system.

The rest of this paper is organized as follows: in Section 2, Caputo fractional-order and Amdomian solutions are introduced into an improved MHNN. In Section 3, the dynamics of FMHNN with different order and coupling strengths are analyzed. Section 4 introduces FMHNN's application in the audio encryption of Internet of Things, and realizes it with Raspberry Pi. Section 5 presents the conclusion of this paper.

2. Description of the FMHNN

2.1. Caputo Fractional-Order Derivative and ADM

Captor fractional derivative is one of the generalizations of integer derivative, the definition of the Caputo fractional-order derivative is given by:

$$ {}^{*}D_{t_0}^{q} f(t) = \begin{cases} \frac{1}{\Gamma(m-q)} \int_0^t \frac{f(m)(\tau)}{(t-\tau)^{q+1-m}} d\tau, m-1 < q < m \\ \frac{d^m}{dt^m} f(t), q = m, \end{cases} \tag{1} $$

where the Gamma function is $\Gamma(\alpha) = \int_0^{+\infty} t^{\alpha-1} e^{-1} dt$, and ${}^{*}D_{t_0}^{q} x(t)$ is the Caputo derivative operator with order q.

For a given fraction-order chaotic system ${}^{*}D_{t_0}^{q} x(t) = f(x(t)) + c(t)$, where $f(x(t))$ represents the function (including linear and nonlinear parts), $[x(t) = [x_1(t), x_2(t), \ldots, x_n(t)]$

are state variables, $c(t)$ is constant. From the Adomian decomposition method (ADM) [47], the system is divided into three parts by the following equation:

$$ {}^{*}D_{t_0}^{q} x(t) = Lx(t) + Nx(t) + x^{k}(t_{t_0}^{+}), \tag{2} $$

where ${}^{*}D_{t_0}^{q} x(t)$ is the Caputo derivative operator with order q, L is the linear part of FMHNN, N is the nonlinear part of FMHNN, $x^{k}(t_{t_0}^{+})$ is initial values. Integrate both sides of Equation (2) to obtain:

$$ x = J_{t_0}^{q} L(x) + J_{t_0}^{q} N(x) + J_{t_0}^{q} g + x^{k}(t_{t_0}^{+}). \tag{3} $$

According to ADM, We use $x = \sum_{i=0}^{\infty} x^{i}$ to represent the solution of the Equation (3). The nonlinear term $N(x)$ can be decomposed as follows:

$$ \begin{cases} A_j^i = \frac{1}{i!}\left[\frac{d^i}{d\lambda^i} N(v_j^i(\lambda))\right]_{\lambda = 0;\ i = 0,1,\cdots,\infty;\ j = 1,\cdots,n} \\ v_j^i(\lambda) = \sum_{k=0}^{i} (\lambda)^k x_j^k. \end{cases} \tag{4} $$

Then the nonlinear term can be expressed as:

$$ N(x) = \sum_{i=0}^{\infty} A^{i}(x^0, x^1, \cdots, x^i). \tag{5} $$

The solution of the equation is:

$$ x = \sum_{i=0}^{\infty} x^{i} = J_{t_0}^{q} \sum_{i=0}^{\infty} L(x^i) + J_{t_0}^{q} \sum_{i=0}^{\infty} A^{i} + J_{t_0}^{q} g + x(t_{t_0}^{+}). \tag{6} $$

The derivation is as follows:

$$ \begin{aligned} x^0 &= J_{t_0}^{q} g + x(t_{t_0}) \\ x^1 &= J_{t_0}^{q} \sum_{i=0}^{\infty} L(x^0) + J_{t_0}^{q} A^0(x^0) \\ x^2 &= J_{t_0}^{q} \sum_{i=0}^{\infty} L(x^1) + J_{t_0}^{q} A^1(x^0, x^1) \\ &\cdots \\ x^i &= J_{t_0}^{q} \sum_{i=0}^{\infty} L(x^{i-1}) + J_{t_0}^{q} A^{i-1}(x^0, x^1, \cdots, x^{i-1}). \end{aligned} \tag{7} $$

2.2. The FMHNN Model

A general HNN formulation can be defined as:

$$ \dot{x} = -x + W \tanh(x), \tag{8} $$

where the neuron state variable is expressed as $x = [x_1(t), x_2(t), x_3(t)]^T$, the nonlinear neuron activation function is expressed as $\tanh(x) = [\tanh(x_1), \tanh(x_2), \tanh(x_3)]^T$, and the weight matrix representing the relationship between neurons is expressed as W.

In [50], a new memristor $\varphi(w) = a + bh(w)$ is proposed, which can generate multi-scroll attractors, where $h(w) = w - \sum_{i=1}^{N} \mathrm{sgn}(w + (2i-1)) + \mathrm{sgn}(w - (2i-1))$, $N = 1, 2, 3, \ldots$. In order to obtain more accurate numerical simulation results, we replaced the sgn function with tanh. The new MHNN replaces the second neuron's synaptic weight with memristor; the topology of the new MHNN is shown in Figure 1 and the MHNN model can be expressed as:

$$\begin{cases} \dot{x} = -x + w_{11}\tanh(x) + w_{12}\tanh(y) + w_{13}\tanh(z) \\ \dot{y} = -y + w_{21}\tanh(x) + k\varphi(w)\tanh(y) + w_{23}\tanh(z) \\ \dot{z} = -z + w_{31}\tanh(x) + w_{32}\tanh(y) + w_{33}\tanh(z) \\ \dot{w} = c\tanh(y) - \mathrm{d}h(w), \end{cases} \tag{9}$$

where a, b, c, d are the parameters of memristor, x, y, z, w are the state variables of the system, k is coupling strength, and the synaptic matrix w can be described as follows:

$$W = \begin{bmatrix} 2.2 & -1.2 & 0.5 \\ 2 & k\varphi(w) & 1.15 \\ -5 & 0 & -1 \end{bmatrix} \tag{10}$$

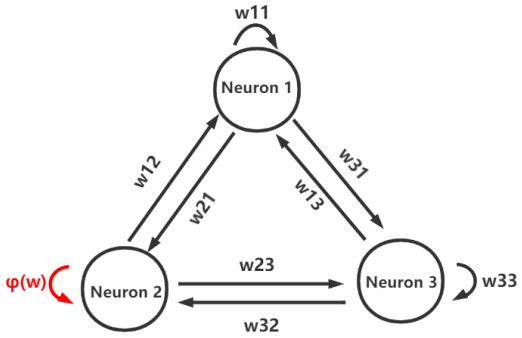


Figure 1. Topological connection of FMHNN.

According to the definition of Caputo fractional-order from Equation (1), the FMHNN can be described as:

$$\begin{cases} {}_{t_0}D_t^q x = -x + 2.2\tanh(x) - 1.2\tanh(y) + 0.5\tanh(z) \\ {}_{t_0}D_t^q y = -y + 2\tanh(x) + k(a + bh(w))\tanh(y) + 1.15\tanh(z) \\ {}_{t_0}D_t^q z = -z + -5\tanh(x) - 1\tanh(z) \\ {}_{t_0}D_t^q w = c\tanh(y) - \mathrm{d}h(w), \end{cases} \tag{11}$$

where ${}_{t_0}D_t^q$ is Caputo fractional calculus operator, q is the order of FMHNN, t_0 is the lower limit of integration, and t is the upper limit of the integral.

In order to find the equilibrium point of the system, let ${}_{t_0}D_t^q x = 0$, ${}_{t_0}D_t^q y = 0$, ${}_{t_0}D_t^q z = 0$, ${}_{t_0}D_t^q w = 0$, $a = 1, b = 0.03, c = 3, d = 1.3, N = 2$, and the following equation can be obtained:

$$\begin{cases} 0 = -x + 2.2\tanh(x) - 1.2\tanh(y) + 0.5\tanh(z) \\ 0 = -y + 2\tanh(x) + k(a + bh(w))\tanh(y) + 1.15\tanh(z) \\ 0 = -z + -5\tanh(x) - 1\tanh(z) \\ 0 = c\tanh(y) - dh(w). \end{cases} \tag{12}$$

We simplify x and y in Equation (12), and obtain the equations as follows:

$$\begin{cases} x = a\tanh((z + \tanh(z))/5) \\ y = a\tanh(1.3 * h(w)/3), \end{cases} \tag{13}$$

where $h(w) = w - \mathrm{sgn}(w-1) - \mathrm{sgn}(w+1) - \mathrm{sgn}(w-3) - \mathrm{sgn}(w+3)$, the equilibrium point can be solved by substituting it into z and w of the Equation (12). We can obtain two types of equilibria: three unstable index-1 saddle-focus and 12 unstable index-2 saddle-focus.

The corresponding eigenvalues can be obtained from the Jacobian matrix:

$$J = \begin{bmatrix} -1 + 2.2sech^2(x) & -1.2sech^2(y) & 0.5sech^2(z) & 0 \\ 2sech^2(x) & -1 + ku(w)sech^2(y) & 1.15sech^2(z) & ku'(w)\tanh(y) \\ -5sech^2(x) & 0 & -1 - sech^2(z) & 0 \\ 0 & 3sech^2(y) & 0 & -1.3h'(w) \end{bmatrix} \quad (14)$$

We can obtain 15 saddle-focus altogether; the unstable index-1 saddle-focus are $(0, 0, 0, \pm 1)$, $(0, 0, 0, \pm 2)$, $(0, 0, 0, \pm 4)$, of which the corresponding eigenvalues are $\lambda_1 = -1.3$, $\lambda_2 = 0.7463$ and $\lambda_{3,4} = -0.5232 \pm 1.615i$. On the other hand, the unstable index-2 saddle-focus are (0.56, 0.083, −1.566, −3.809), (0.56, 0.083, −1.566, −1.809), (0.56, 0.083, −1.566, 0.191), (0.56, 0.083, −1.566, 2.191), (0.56, 0.083, −1.566, 4.191), of which the eigenvalues are $\lambda_1 = -0.837$, $\lambda_2 = -1.303, \lambda_{3,4} = 0.405 \pm 1.255i$. The rest of the unstable index-2 saddle-focus are (−0.56, −0.083, 1.566, 3.809), (−0.56, −0.083, 1.566, 1.809), (−0.56, −0.083, 1.566, −0.191), (−0.56, −0.083, 1.566, −2.191), (−0.56, −0.083, 1.566, −4.191), of which the eigenvalues are $\lambda_1 = -0.833$, $\lambda_2 = -1.297$, $\lambda_{3,4} = 0.392 \pm 1.259i$.

Shil'nikov's theorem [51] shows that, when the nonlinear system in a real root γ and two conjugate complex $\sigma \pm j\omega$ satisfy the $|\sigma/\gamma| < 1$ and $\sigma\gamma < 0$, the system is chaotic. It can be seen from the results that the eigenvalues of the equilibrium points above meet the conditions, which basically proves the chaotic characteristics of the system.

3. Dynamics Analysis and Numerical Simulations

3.1. Phase Portraits of Multi-Scroll with Different Parameter

Compared with ordinary chaotic attractors, multi-scroll chaotic attractors have more complex dynamics and more key parameters, which is especially important for audio encryption applications with high security requirements. We can fix the parameters as $q = 0.98$, $a = 1, b = 0.03, c = 3, d = 1.3$, $N = 2$. When and $k = 1.32$, the system presents one-scroll chaotic attractors as shown in Figure 2. When we change the coupling strength k =1.6, the system presents double-scroll attractors as shown in Figure 3. From Figure 4, we found that the number of double-scroll can also be controlled by memristor. When $N = 1$, $N = 2$, $N = 3$, the number of double-scroll is 1, 5, and 7 respectively. This indicates the existence of multi-scroll attractors in the system.

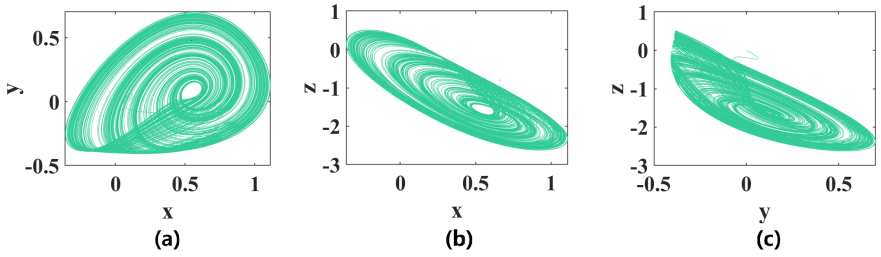


Figure 2. Phase portraits with $q = 0.98$, $k = 1.32$. (**a**) x-y plane ; (**b**) x-z plane; (**c**) y-z plane.

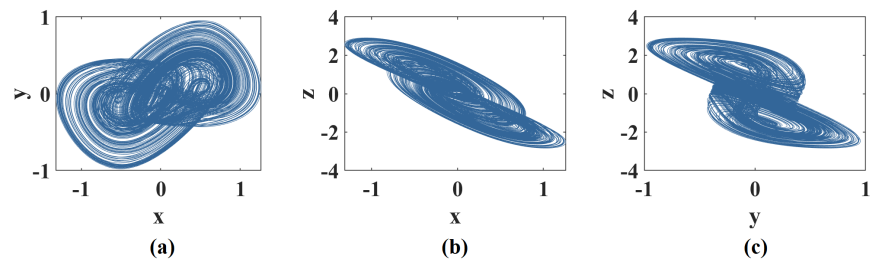


Figure 3. Phase portraits with $q = 0.98$, $k = 1.6$. (**a**) x-y plane ; (**b**) x-z plane; (**c**) z-w plane.

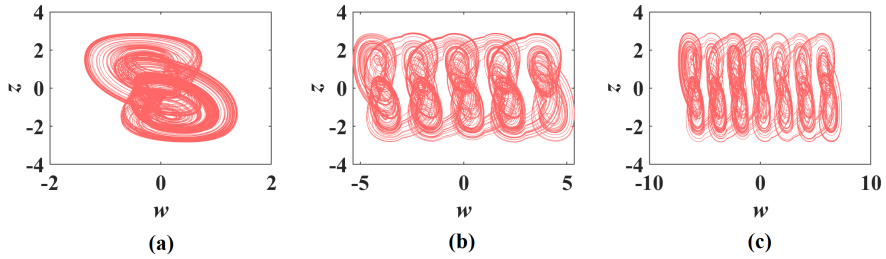


Figure 4. Multi-scroll attractors with different parameters in w-z plane. (**a**) $N = 1$; (**b**) $N = 2$; (**c**) $N = 3$.

3.2. Bifurcation of FMHNN with Different Parameters

3.2.1. Bifurcation with Synaptic Coupling Strength k

The parameters of FMHNN in this part are given by $q = 0.98$, $a = 1, b = 0.03$, $c = 3$, $d = 1.3, N = 2$. The bifurcation variation characteristics of the system with coupling parameter k are shown in Figure 5. When the coupling parameter k is between 1.1 and 1.25, the system is in a periodic state; when the coupling parameter k is between 1.3 and 1.48, the system is in the coexistence of cycle and chaos, and gradually transforms into complex chaos. When k is between 1.48 and 1.6, the system is in a counter-periodic state, and the system degenerates from chaos to coexistence of period and chaos. When k is between 1.6 and 1.9, the system enters the complex chaotic state again, which also contains a small part of the periodic state. It can be seen that the system has a wide range of chaotic state intervals.

3.2.2. Bifurcation with Different Order q

When the coupling parameter $k = 1.9$ is selected, the bifurcation variation characteristics of the system with order q are shown in Figure 6. When q is between 0.8 and 0.85, the system is in a periodic state; when q is between 0.85 and 0.89, the system enters a chaotic state. With the increase of order q, the system will enter a reverse periodic state. When the order q is between 0.91 and 0.97, the system enters a complex chaotic state. It can be seen that the system has a chaotic state that changes with order q and has excellent chaotic characteristics.

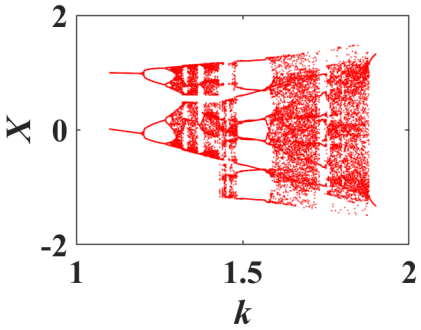


Figure 5. Bifurcation diagrams with $q = 0.98$, $k \in (1, 2)$.

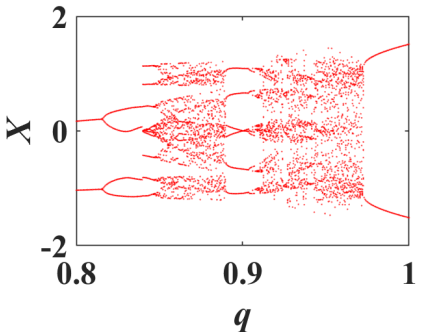


Figure 6. Bifurcation diagrams with $k = 1.9$, $q \in (0.8, 1)$.

3.3. Multiple Coexisting Attractors and Basins of Attractor

Multiple coexistence of attractor is a special phenomenon in the nonlinear system; the system can generate multiple attractors to coexist by changing the initial conditions. Multiple stability is the intrinsic characteristics of many nonlinear dynamic systems, and the result of the coexistence of many of the attractors. In a nutshell, if a system has multiple attractors and the external excitation is strong enough to switch states, it should be multi-stable [52].

The coexistence of attractors can be observed through the x-z plane when $q = 0.98$, $a = 1, b = 0.03, c = 3, d = 1.3, N = 2$ are given. We select two sets of initial values $(-0.1, 0, 0, 0)$ and $(0.1, 0, 0, 0)$, symmetric about the origin $(0, 0, 0, 0)$. As shown in Figure 7, the synaptic coupling strengths are k = 1.2, 1.3 and 1.4 respectively, which can produce abundant chaotic attractor coexistence phenomena, including chaotic and chaotic coexistence, periodic and chaotic coexistence, and periodic and periodic coexistence. Meanwhile, the basins of attraction are shown in Figure 8. Because of the rich characteristics of chaos, it has rich applications and great research value for information security, secure communication and other fields.

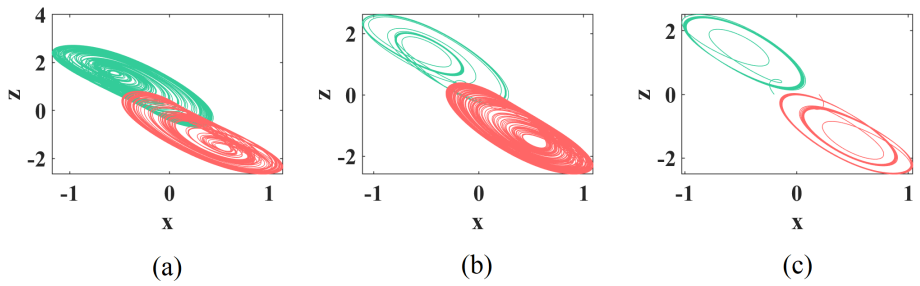


Figure 7. The coexistence of attractors in x-z plane. (**a**) k = 1.4, (**b**) k = 1.3, (**c**) k = 1.2.

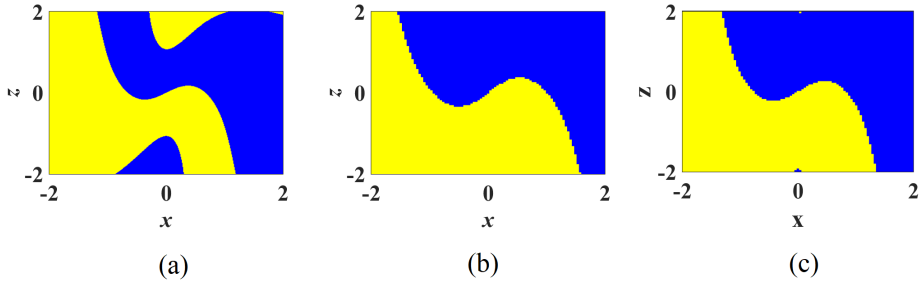


Figure 8. The basins of attraction in x-z plane. (**a**) k = 1.4, (**b**) k = 1.3, (**c**) k = 1.2.

4. Audio Encryption Application in IoT under MQTT Protocol

With the popularity of networked devices and cloud computing, it is possible for ten billion devices to be connected through the Internet. In the modern society with the continuous development of the Internet, the Internet of Things (IoT) has brought new development opportunities and challenges to the information society. On the IoT, people will transfer a large amount of information, and a lot of data and equipment may become the target of cyberattacks. How to ensure security and privacy in the IoT and the Industrial Internet of Things (IIoT) is related to network reliability and network security [53–55]. Due to the initial value sensitivity, randomness and unpredictability of chaotic systems, image encryption [56–62], random number generator [63–65] and secure communication [66–70] based on chaos have become popular research hotspots in the field of information security.

This part introduces the audio encryption application of the FMHNN model in Smart Home scenario as shown in Figure 9—the audio encryption system based on the MQTT protocol, which is a lightweight transmission protocol based on client-server message publishing/subscription. That is to say, if multiple devices need to receive the same

message at the same time, they can agree on a channel with the sender, the sender will send the message to the server through this channel, and then the server will distribute it to the receivers who subscribe to this channel. The biggest advantage of MQTT is that it can provide real-time and reliable message services for multiple remote devices with very little code and limited bandwidth. As a low-overhead, low-bandwidth instant messaging protocol, the MQTT protocol is widely used in IoT, smart home, and mobile applications.

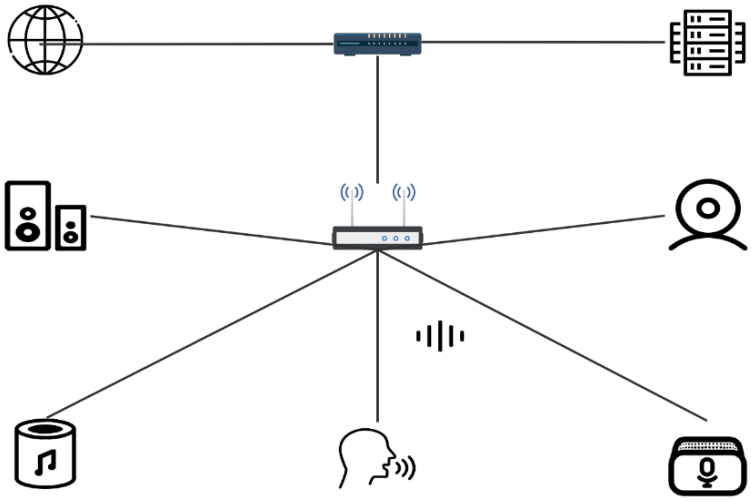


Figure 9. Secure Audio Encryption Application in Smart home.

The topology structure of a simple IoT scenario based on the MQTT protocol is shown in Figure 10. Alice, as the sender (Publisher), sends messages to the Broker. Bob, Carol, and Eve as the receivers (Subscribers) can subscribe to different channels (Topic) and receive messages from their respective channels. For example, both Eve and Carol can receive "AUDIO" data, only Carol can restore the audio normally, Eve cannot obtain the correct key to restore the audio because he has not previously subscribed to the 'KEY' channel.

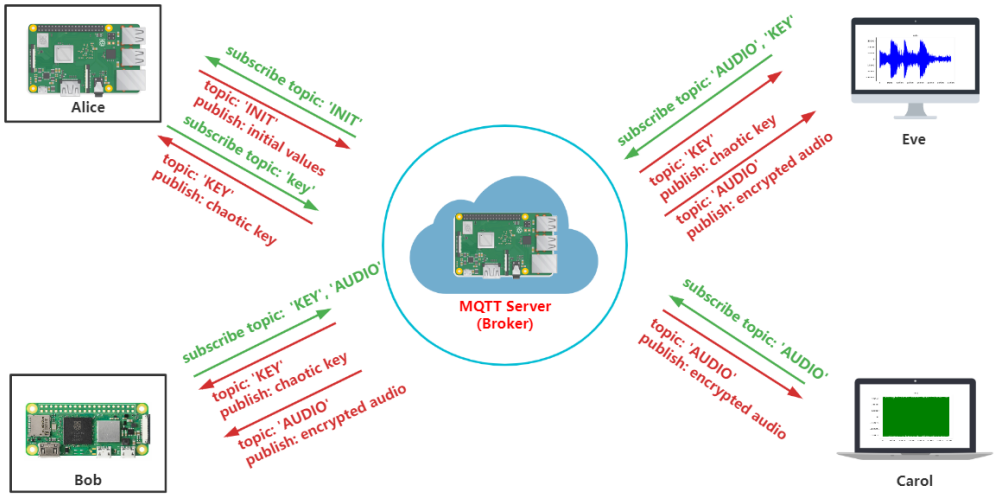


Figure 10. Topology structure of IoT Application under MQTT protocol.

We adopted three new measures to increase the system's security and real-time performance. Firstly, due to the limited computing power of edge devices and the high complexity of the chaotic key generation algorithm, we were inspired by cloud computing and placed the key generation module on the high-performance Broker Server, which is distributed by the Broker Server through a specific channel, so that the time of encryption and decryption is greatly shortened. At the same time, we adopted a one-time key, so that the key for each

audio encryption is different, which greatly improves the security of the data. Furthermore, the security of each channel name is equally important, so we chose the SHA256 algorithm to hash each topic, as shown in Table 1, so that the messages of each channel cannot be distinguished by the attacker.

Table 1. Topics after SHA256 algorithm processing.

Topic	After SHA256
KEY	2c70e12b7a0646f92279f427c7b38e7334d8e5389cff167a1dc30e73f826b683
INIT	bb54068aea85faa7e487530083366be9962390af822e4c71ef1aca7033c83e66
AUDIO	6ed8919ce20490a5e3ad8630a4fab69475297abd07db73918dd5f36fcfaeb11b

The flow chart of the message subscription and publishing is shown in Figure 11. The Publisher represents Alice as the sender, the Broker represents the Server and Eve as the relay station and eavesdropper, and the Subscriber represents Bob as the receiver. First, the Publisher sends the initial value to the Broker Server in the 'INIT' channel. The Broker Server obtains a chaotic key from FMHNN, and distributes it to Publishers and Subscribers through the 'KEY' channel. After the Publisher receives the key, it starts to encrypt the audio and publish the encrypted audio in 'AUDIO' channel. After the Subscriber receives the data from the subscribed 'AUDIO' channel, it decrypts the encrypted data with the one-time key received before restoring the original audio.

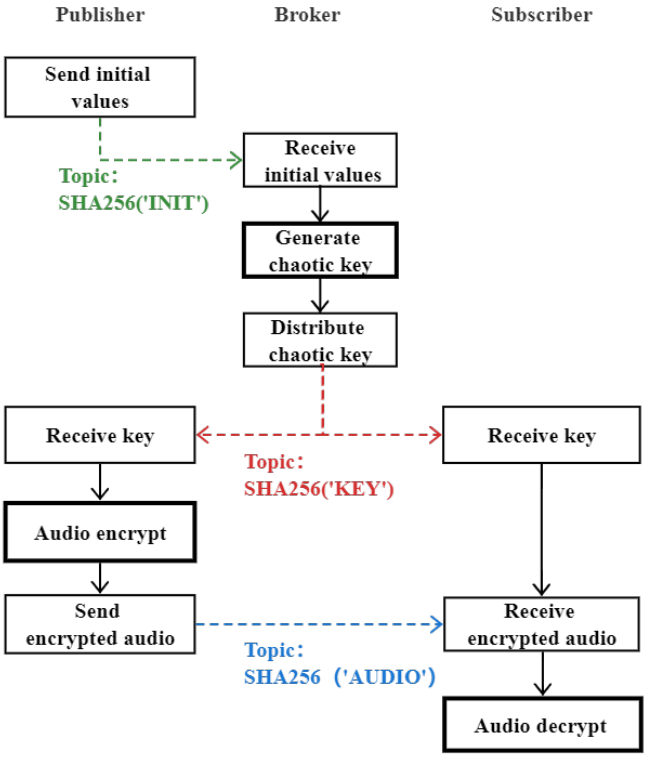


Figure 11. Flow chart of audio encrypt process.

The system uses Python3.7 for development, uses 'emqx' as the implementation of the MQTT protocol, and deploys on Docker. The system is divided into three subsystems: sender, receiver and server, as shown in Figure 12 in the left project structure bar. Each subsystem is divided into main program and toolkit, among which 'plot.py' and 'sha256.py' are general modules, playing the functions of display and confusion Topic respectively. The unique module of subsystem Publisher is 'encrypt.py', the unique module of subsystem Broker is 'keygen.py', and the unique module of Subscriber is 'decrypt.py'. Part of the code is shown in Figure 12.

In order to simulate the real application scenario, we established a typical LAN composed of three devices, as shown in Figure 13. in which the sender and receiver are two Raspberry Pis with limited computing power, and the server is a high-performance laptop. The IP address of each device is shown in Table 2. In order to display the experimental effect, we used VNC Viewer to remotely connect to each Raspberry Pi. You can see the original audio sent by Alice as shown in Figure 14. In this experiment, the Server also acts as the role of Eve as the attacker. We can perceive the excellent encryption effect from the spectrum diagram as shown in Figure 15. The audio obtained by Bob as the receiver after decryption is shown in Figure 16, corresponding to the effect of Figure 13 in turn, which well restores the original audio and realizes a complete confidential communication.

Table 2. IP address and role of each device.

Device	Role	IP Adress
Raspberry Pi 1	Publisher Alice	192.168.137.149
Laptop	Broker Server&Eve	192.168.137.1
Raspberry Pi 2	Subscriber Bob	192.168.137.174

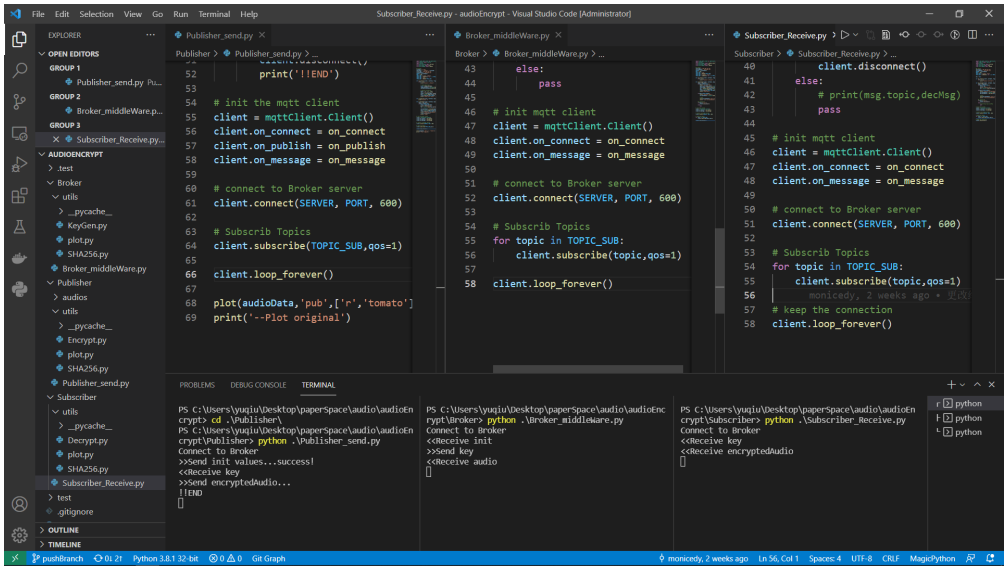


Figure 12. Code of Audio encryption by MQTT, left part is Publisher, middle part is Broker, right part is Subscriber.

We compare this paper with some typical chaotic encryption schemes; the results are shown in Table 3. From the perspective of the encryption system, the system used in this paper has the advantages of multi scroll and fractional order, which will help to generate more complex keys. From the point of view of main encryption technologies, the system adopts the technology of combining cloud computing with the MQTT protocol. Compared with simple pseudo-random number generator (PRNG) technology, cloud computing technology shortens the time of data encryption, and MQTT technology improves the security and reliability of data transmission. In terms of encrypted data objects, audio encryption is an important field that cannot be ignored at present. This paper provides a good solution for voice control in the field of Internet of things. Finally, in terms of practical application scenarios, the low price makes Raspberry Pi more suitable as one of the countless nodes of the Internet of Things. Compared with traditional DSP and FPGA, Raspberry Pi supports multiple development languages, which greatly improves the development efficiency of the encryption system. So the audio encryption scheme under cloud MQTT is a very ideal voice control solution for the Internet of Things.

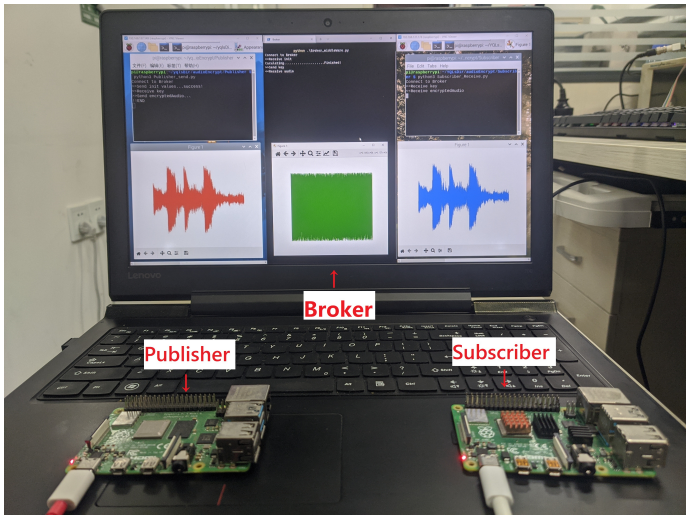


Figure 13. Raspberry Pi 1 as Publisher, Laptop as Broker, Raspberry Pi 2 as Subscriber.

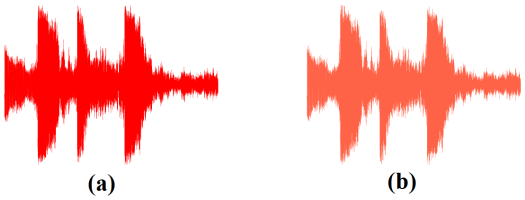


Figure 14. The original audio before publish. (**a**) left channel, (**b**) right channel.

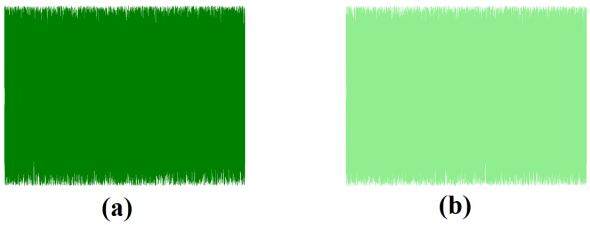


Figure 15. The audio that has been encrypted with FMHNN. (**a**) left channel, (**b**) right channel.

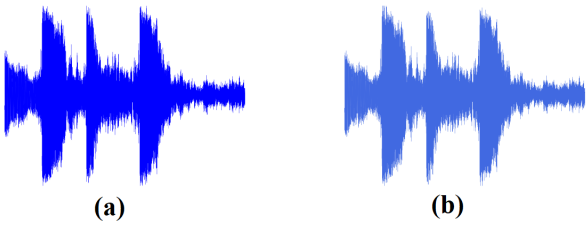


Figure 16. The audio decrypted by Topic "KEY". (**a**) left channel, (**b**) right channel.

Table 3. Comparison with previous work.

Reference	System	Main Technique	Data Type	Implemented Device	Cost of Large-Scale Deployment	Difficulty of Implementation
Ref. [19]	Ordinary memristive Hopfield neural network	PRNG	Picture	FPGA	High	High
Ref. [53]	Multiple different systems	Local MQTT	Picture	Raspberry Pi	Low	Low
Ref. [71]	Logistic map	Double K-L transformation algorithm	Picture	DSP	Low	High
This paper	Multi-scroll fractional-order memristive hopfield neural network	Cloud MQTT	Audio	Raspberry Pi and high-performance Server	Low	Low

5. Conclusions

This work investigated a multi-scroll fractional-order memristive hopfield neural network. By studying the coupling strength of memristor and the order of FMHNN, it is found that the system presents abundant dynamic phenomena such as multiple coexisting attractors and bifurcation; besides, we can also generate multi-scroll by changing parameters of the memristor. Furthermore, we developed an audio encryption scheme for IoT based on the concept of cloud computing, and implemented this encryption system on Raspberry Pi programming by Python. We managed the most complex computing process (such as a chaotic key generation algorithm) on a high-performance cloud server, so as to convert the computing complexity into network delay, which illustrates the importance of network reliability and security from another perspective, and the MQTT protocol in this paper solved this problem. The results show that FMHNN has broad application prospects in the Internet of Things and smart home scenarios.

Research shows that multi-delays usually exist in signal transmission in fractional-order neural networks, so multi-delays will affect various dynamic behaviors of fractional-order neural networks [72–77]. Our next main work is to study the stability and bifurcation of fractional-order neural networks in the case of multi-delays, and the application of fractional-order neural networks with multi-delays in IoT.

Author Contributions: Conceptualization, F.Y. and Q.Y.; methodology, Q.Y.; software, F.Y.; validation, Q.Y., H.C. and X.K.; formal analysis, Q.Y.; investigation, S.D.; resources, F.Y.; data curation, Q.Y.; writing—original draft preparation, Q.Y.; writing—review and editing, F.Y. and A.A.M.M.; visualization, S.C.; supervision, F.Y.; project administration, F.Y. and S.C.; funding acquisition, F.Y., S.C. and S.D. All authors have read and agreed to the published version of the manuscript.

Funding: This paper was supported by the Natural Science Foundation of Hunan Province under Grants 2022JJ30624 and 2022JJ10052, the Scientific Research Fund of Hunan Provincial Education Department under grant 21B0345, the National Natural Science Foundation of China under Grant 62172058, the special funds for the construction of innovative provinces in Hunan Province under Grants 2020JK4046 and 2022SK2007, and the Changsha Science and Technology Project under Grant KH2202001.

Institutional Review Board Statement: Not applicable.

Informed Consent Statement: Not applicable.

Data Availability Statement: All the data were computed using our algorithms.

Acknowledgments: The authors would like to thank the editors and reviewers for their selfless dedication, which has greatly improved the quality of the paper!

Conflicts of Interest: The author declares no conflict of interest. The funder had no role in the design of the study; in the collection, analyses, or interpretation of data; in the writing of the manuscript, or in the decision to publish the results.

References

1. Yang, L.; Wang, C. Emotion model of associative memory possessing variable learning rates with time delay. *Neurocomputing* **2021**, *460*, 117–125. [CrossRef]
2. Leung, K.S.; Jin, H.D.; Xu, Z.B. An expanding self-organizing neural network for the traveling salesman problem. *Neurocomputing* **2004**, *62*, 267–292. [CrossRef]
3. Cheng, L.; Liu, W.; Hou, Z.G.; Yu, J.; Tan, M. Neural-network-based nonlinear model predictive control for piezoelectric actuators. *IEEE Trans. Ind. Electron.* **2015**, *62*, 7717–7727. [CrossRef]
4. Yu, F.; Liu, L.; Xiao, L.; Li, K.; Cai, S. A robust and fixed-time zeroing neural dynamics for computing time-variant nonlinear equation using a novel nonlinear activation function. *Neurocomputing* **2019**, *350*, 108–116. [CrossRef]
5. Wang, J.; Wu, Y.; He, S.; Sharma, P. K.; Yu, X.; Alfarraj, O.; Tolba, A. Lightweight Single Image Super-Resolution Convolution Neural Network in Portable Device. *KSII Trans. Internet Inf. Syst.* **2021**, *15*, 4065–4083.
6. Deng, Z.; Zhu, Q.; He, P.; Zhang, D.; Luo, Y. A Saliency Detection and Gram Matrix Transform-Based Convolutional Neural Network for Image Emotion Classification. *Secur. Commun. Netw.* **2021**, *2021*, 6854586. [CrossRef]
7. Long, M.; Zeng, Y. Detecting iris liveness with batch normalized convolutional neural network. *CMC-Comput. Mater. Contin.* **2019**, *58*, 493–504. [CrossRef]

8. Gui, Y.; Zeng, G. Joint learning of visual and spatial features for edit propagation from a single image. *Vis. Comput.* **2020**, *36*, 469–482. [CrossRef]
9. Zhou, S.; Tan, B. Electrocardiogram soft computing using hybrid deep learning CNN-ELM. *Appl. Soft Comput.* **2020**, *86*, 105778. [CrossRef]
10. Wang, J.; Zou, Y.; Lei, P.; Sherratt, R. S.; Wang, L. Research on recurrent neural network based crack opening prediction of concrete dam. *J. Internet Technol.* **2020**, *21*, 1161–1169.
11. Lin, H.; Wang, C.; Deng, Q.; Xu, C.; Deng, Z.; Zhou, C. Review on chaotic dynamics of memristive neuron and neural network. *Nonlinear Dyn.* **2021**, *106*, 959–973. [CrossRef]
12. Yu, F.; Shen, H.; Zhang, Z.; Huang, Y.; Cai, S.; Du, S. Dynamics analysis, hardware implementation and engineering applications of novel multi-style attractors in a neural network under electromagnetic radiation. *Chaos Solitons Fractals* **2021**, *152*, 111350. [CrossRef]
13. Liao, M.; Wang, C.; Sun, Y.; Lin, H.; Xu, C. Memristor-based affective associative memory neural network circuit with emotional gradual processes. *Neural Comput. Appl.* **2022**. [CrossRef]
14. Tlelo-Cuautle, E.; González-Zapata, A.M.; Díaz-Muñoz, J.D.; de la Fraga, L.G.; Cruz-Vega, I. Optimization of fractional-order chaotic cellular neural networks by metaheuristics. *Eur. Phys. J. Spec. Top.* **2022**, 1–7. [CrossRef]
15. Xu, Q.; Ju, Z.; Ding, S.; Feng, C.; Chen, M.; Bao, B. Electromagnetic induction effects on electrical activity within a memristive Wilson neuron model. *Cogn. Neurodyn.* **2022**. [CrossRef]
16. Xu, C.; Wang, C.; Sun, Y.; Hong, Q.; Deng, Q.; Chen, H. Memristor-based neural network circuit with weighted sum simultaneous perturbation training and its applications. *Neurocomputing* **2021**, *462*, 581–590. [CrossRef]
17. Yu, F.; Zhang. Z.; Shen, H.; Huang, Y.; Cai, S.; Jin, J.; Du, S. Design and FPGA implementation of a pseudo-random number generator based on a Hopfield neural network under electromagnetic radiation. *Front. Phys.* **2021**, *9*, 690651. [CrossRef]
18. Ju, Z.; Lin, Y.; Chen, B.; Wu, H.; Chen, M.; Xu, Q. Electromagnetic radiation induced non-chaotic behaviors in a Wilson neuron model. *Chin. J. Phys.* **2022**, *77*, 214–222. [CrossRef]
19. Yu, F.; Zhang, Z.; Shen, H.; Huang, Y.; Cai, S.; Du, S. FPGA implementation and image encryption application of a new PRNG based on a memristive Hopfield neural network with a special activation gradient. *Chin. Phys. B* **2022**, *31*, 020505. [CrossRef]
20. Yao, W.; Wang, C.; Sun, Y.; Zhou, C. Robust multimode function synchronization of memristive neural networks with parameter perturbations and time-varying delays. *IEEE Trans. Syst. Man Cybern. Syst.* **2020**, *52*, 260–274. [CrossRef]
21. Yu, F.; Chen, H.; Kong, X.; Yu, Q.; Cai, S.; Huang, Y.; Du, S. Dynamic analysis and application in medical digital image watermarking of a new multi-scroll neural network with quartic nonlinear memristor. *Eur. Phys. J. Plus* **2022**, *350*, 108–116. [CrossRef] [PubMed]
22. Xu, Q.; Lin, Y.; Bao, B.; Chen, M. Multiple attractors in a non-ideal active voltage-controlled memristor based Chua's circuit. *Chaos Solitons Fractals* **2016**, *83*, 186–200. [CrossRef]
23. Ma, X.; Mou, J.; Liu, J.; Ma, C.; Yang, F.; Zhao, X. A novel simple chaotic circuit based on memristor-memcapacitor. *Nonlinear Dyn.* **2020**, *100*, 2859-2876. [CrossRef]
24. Xu, C.; Wang, C.; Jiang, J.; Sun, J.; Lin, H. Memristive Circuit Implementation of Context-Dependent Emotional Learning Network and Its Application in Multi-Task. *IEEE Trans.-Comput.-Aided Des. Integr. Circuits Syst.* **2021**. [CrossRef]
25. Xu, Q.; Cheng, S.; Ju, Z.; Chen, M.; Wu, H. Asymmetric coexisting bifurcations and multi-stability in an asymmetric memristive diode-bridge-based jerk circuit. *Chin. J. Phys.* **2021**, *70*, 69–81. [CrossRef]
26. Lin, H.; Wang, C.; Cui, L.; Sun, Y.; Xu, C.; Yu, F. Brain-like initial-boosted hyperchaos and application in biomedical image encryption. *IEEE Trans. Ind. Inform.* **2022**. [CrossRef]
27. Wen, Z.; Li, Z.; Li, X. Transient MMOs in memristive chaotic system via tiny perturbation. *Electron. Lett.* **2020**, 56, 78–80. [CrossRef]
28. Wan, Q.; Yan, Z.; Li, F.; Liu, J.; Chen, S. Multistable dynamics in a Hopfield neural network under electromagnetic radiation and dual bias currents. *Nonlinear Dyn.* **2022**, *2022*, 1–17. [CrossRef]
29. Anbalagan, P.; Ramach, ran, R.; Alzabut, J.; Hincal, E.; Niezabitowski, M. Improved Results on Finite-Time Passivity and Synchronization Problem for Fractional-Order Memristor-Based Competitive Neural Networks: Interval Matrix Approach. *Fractal Fract.* **2022**, *6*, 36. [CrossRef]
30. Yu, F.; Li, L.; He, B.; Liu, L.; Qian, S.; Zhang, Z.; Li, Y. Pseudorandom number generator based on a 5D hyperchaotic four-wing memristive system and its FPGA implementation. *Eur. Phys. J.-Spec. Top.* **2021**, *230*, 1763–1772. [CrossRef]
31. Wen, Z.; Li, Z.; Li, X. Bursting dynamics in parametrically driven memristive Jerk system. *Chin. J. Phys.* **2020**, *66*, 327–334. [CrossRef]
32. Petras, I. Oscillators Based on Fractional-Order Memory Elements. *Fractal Fract.* **2022**, *6*, 283. [CrossRef]
33. Zidan, M.A.; Fahmy, H.A.H.; Hussain, M.M.; Salama, K.N. Memristor-based memory: The sneak paths problem and solutions. *Microelectron. J.* **2013**, *44*, 176–183. [CrossRef]
34. Mohammad, B.; Homouz, D.; Elgabra, H. Robust Hybrid Memristor-CMOS Memory: Modeling and Design. *IEEE Trans. Very Large Scale Integr. VLSI Syst.* **2013**, *21*, 2069–2079. [CrossRef]
35. Chang, T.; Jo, S.H.; Lu, W. Short-term memory to long-term memory transition in a nanoscale memristor. *ACS Nano* **2011**, *5*, 7669–7676. [CrossRef] [PubMed]

36. Yao, W.; Wang, C.; Cao, J.; Sun, Y.; Zhou, C. Hybrid multisynchronization of coupled multistable memristive neural networks with time delays. *Neurocomputing* **2019**, *363*, 281–294. [CrossRef]
37. Yao, W.; Wang, C.; Sun, Y.; Zhou, C.; Lin, H. Synchronization of inertial memristive neural networks with time-varying delays via static or dynamic event-triggered control. *Neurocomputing* **2020**, *39*, 367–380. [CrossRef]
38. Thomas, A. Memristor-based neural networks. *J. Phys. D Appl. Phys.* **2013**, *46*, 093001. [CrossRef]
39. Zhou, C.; Wang, C.; Sun, Y.; Yao, W. Weighted sum synchronization of memristive coupled neural networks. *Neurocomputing* **2020**, *403*, 225–232. [CrossRef]
40. Lin, H.; Wang, C; Yao, W.; Tan, Y. Chaotic dynamics in a neural network with different types of external stimuli. *Commun. Nonlinear Sci. Numer. Simul.* **2020**, *90*, 105390. [CrossRef]
41. Han, X.; Hymavathi, M.; Sanober, S.; Dhupia, B.; Syed Ali, M. Robust stability of fractional order memristive BAM neural networks with mixed and additive time varying delays. *Fractal Fract.* **2022**, *6*, 62. [CrossRef]
42. Tan, Y.; Wang, C. A simple locally active memristor and its application in HR neurons. *Chaos* **2020**, *30*, 053118. [CrossRef] [PubMed]
43. Xu, Q; Liu, T; Feng, C.; Bao, H.; Wu, H.; Bao, B. Continuous non-autonomous memristive Rulkov model with extreme multistability. *Chin. Phys. B* **2021**, *30*, 128702. [CrossRef]
44. Chen, C.; Min, F.; Zhang, Y.; Bao, B. Memristive electromagnetic induction effects on Hopfield neural network. *Nonlinear Dyn.* **2021**, *106*, 2559–2576. [CrossRef]
45. Li, X.; Mou, J.; Cao, Y.; Banerjee, S. An Optical Image Encryption Algorithm Based on a Fractional-Order Laser Hyperchaotic System. *Int. J. Bifurc. Chaos* **2022**, *32*, 2250035. [CrossRef]
46. Song, C.; Cao, J. Dynamics in fractional-order neural networks. *Neurocomputing* **2014**, *142*, 494–498. [CrossRef]
47. Ma, C.; Mou, J.; Yang, F.; Yan, H. A fractional-order hopfield neural network chaotic system and its circuit realization. *Eur. Phys. J. Plus* **2020**, *135*, 100. [CrossRef]
48. Fan, Y.; Huang, X.; Wang, Z.; Li, Y. Nonlinear dynamics and chaos in a simplified memristor-based fractional-order neural network with discontinuous memductance function. *Nonlinear Dyn.* **2018**, *93*, 611–627. [CrossRef]
49. Yu, F.; Kong, X.; Chen, H.; Yu, Q.; Cai, S.; Huang, Y.; Du, S. A 6D Fractional-Order Memristive Hopfield Neural Network and its Application in Image Encryption. *Front. Phys.* **2022**, *10*, 847385. [CrossRef]
50. Zhang, S.; Zheng, J.; Wang, X.; Zeng, Z.; He, S. Initial offset boosting coexisting attractors in memristive multi-double-scroll Hopfield neural network. *Nonlinear Dyn.* **2020**, *102*, 2821–2841. [CrossRef]
51. Silva, C P. Shil'nikov's theorem—A tutorial. *IEEE Trans. Circuits Syst. Fundam. Theory Appl.* **1993**, *40*, 675–682. [CrossRef]
52. Xu, Q.; Tan, X.; Zhu, D.; Bao, H.; Hu, Y.; Bao, B. Bifurcations to bursting and spiking in the Chay neuron and their validation in a digital circuit. *Chaos Solitons Fractals* **2020**, *141*, 110353. [CrossRef]
53. González-Zapata, A.M.; Tlelo-Cuautle, E.; Cruz-Vega, I.; León-Salas, W.D. Synchronization of chaotic artificial neurons and its application to secure image transmission under MQTT for IoT protocol. *Nonlinear Dyn.* **2021**, *104*, 4581–4600. [CrossRef]
54. Siegel, J.E.; Kumar, S.; Sarma, S.E. The future internet of things: Secure, efficient, and model-based. *IEEE Internet Things J.* **2017**, *5*, 2386–2398. [CrossRef]
55. Airehrour, D.; Gutierrez, J.; Ray, S.K. Secure routing for internet of things: A survey. *J. Netw. Comput. Appl.* **2016**, *66*, 198–213. [CrossRef]
56. Cheng, S.; Sun, J.; Xu, C. A color image encryption scheme based on hybrid cascaded chaotic system. *Int. J. Bifurc. Chaos* **2021**, *31*, 2150125. [CrossRef]
57. Deng, J.; Zhou, M.; Wang, C.; Wang, S.; Xu, C. Image segmentation encryption algorithm with chaotic sequence generation participated by cipher and multi-feedback loops. *Multimed. Tools Appl.* **2021**, *80*, 13821–13840. [CrossRef]
58. Yu, F.; Shen, H.; Zhang, Z.; Huang, Y.; Cai, S.; Du, S. A new multi-scroll Chua's circuit with composite hyperbolic tangent-cubic nonlinearity: Complex dynamics, Hardware implementation and Image encryption application. *Integr.-VLSI J.* **2021**, *81*, 71–83. [CrossRef]
59. Zeng, J.; Wang, C.H. A novel hyper-chaotic image encryption system based on particle swarm optimization algorithm and cellular automata. *Secur. Commun. Netw.* **2021**, *2021*, 6675565. [CrossRef]
60. Li, X.J.; Mou, J.; Banerjee, S.; Wang, Z.S.; Cao, Y.H. Design and DSP implementation of a fractional-order detuned laser hyperchaotic circuit with applications in image encryption. *Chaos Solitons Fractals* **2022**, *159*, 112133. [CrossRef]
61. Gao, X.; Mou, J.; Xiong, L.; Sha, Y.; Yan, H.; Cao, Y. A Fast and Efficient Multiple Images Encryption Based on Single Channel Encryption and Chaotic System. *Nonlinear Dyn.* **2022**, *108*, 613–636. [CrossRef]
62. Cheng, G.; Wang, C.; Xu, C. A novel hyper-chaotic image encryption scheme based on quantum genetic algorithm and compressive sensing. *Multimed. Tools Appl.* **2020**, *79*, 29243–29263. [CrossRef]
63. Yong, Y.U.; Jian, G.; Meng-Ru, Y.U.; Gong-Kun, J.I.A.N.G. A Pseudo-random Number Generator Based on Integer Chaotic Map. *J. Beijing Univ. Posts Telecommun.* **2022**, *45*, 58–62.
64. Cang, S.; Kang, Z.; Wang, Z. Pseudo-random number generator based on a generalized conservative Sprott—A system. *Nonlinear Dyn.* **2021**, *104*, 827–844. [CrossRef]
65. Li, S.; Liu, Y.; Ren, F.; Yang, Z. Design of a high throughput pseudo-random number generator based on discrete hyper-chaotic system. *IEEE Trans. Circuits Syst. Ii Express Briefs* **2022**. [CrossRef]

66. Yu, F.; Qian, S.; Chen, X.; Huang, Y.; Liu, L.; Shi, C.; Wang, C. A New 4D Four-Wing Memristive Hyperchaotic System: Dynamical Analysis, Electronic Circuit Design, Shape Synchronization and Secure Communication. *Int. J. Bifurc. Chaos* **2020**, *30*, 2050147. [CrossRef]
67. Zhou, L.; Tan, F.; Li, X.; Zhou, L. A fixed-time synchronization-based secure communication scheme for two-layer hybrid coupled networks. *Neurocomputing* **2021**, *433*, 131–141. [CrossRef]
68. Liu, J.; Zhang, J.; Wang, Y. Secure Communication via Chaotic Synchronization Based on Reservoir Computing. *IEEE Trans. Neural Netw. Learn. Syst.* **2022**. [CrossRef]
69. Li, Y.; Li, Z.; Ma, M.; Wang, M. Generation of grid multi-wing chaotic attractors and its application in video secure communication system. *Multimed. Tools Appl.* **2020**, *79*, 29161–29177. [CrossRef]
70. Kekha Javan, A.A.; Zare, A.; Alizadehsani, R.; Balochian, S. Robust Multi-Mode Synchronization of Chaotic Fractional Order Systems in the Presence of Disturbance, Time Delay and Uncertainty with Application in Secure Communications. *Big Data Cogn. Comput.* **2022**, *6*, 51. [CrossRef]
71. Geng, X.; Du, C.; Ding, Q. Image Encryption System of New Chaotic Algorithm based on DSP. *Second Int. Conf. Instrum. Meas. Comput. Commun. Control* **2012**, *2012*, 614–618.
72. Shi, J; He, K; Fang, H. Chaos, Hopf bifurcation and control of a fractional-order delay financial system. *Math. Comput. Simul.* **2022**, *194*, 348–364. [CrossRef]
73. Xiao, M.; Zheng, W.; Lin, J.; Jiang, G.; Zhao, L.; Cao, J. Fractional-order PD control at Hopf bifurcations in delayed fractional-order small-world networks. *J. Frankl. Inst.* **2017**, *354*, 7643–7667. [CrossRef]
74. Huang, C.; Wang, J.; Chen, X.; Cao, J. Bifurcations in a fractional-order BAM neural network with four different delays. *Neural Netw.* **2021**, *141*, 344–354. [CrossRef]
75. Xu, C.; Zhang, W.; Aouiti, C.; Liu, Z.; Liao, M.; Li, P. Further investigation on bifurcation and their control of fractional-order bidirectional associative memory neural networks involving four neurons and multiple delays. *Math. Methods Appl. Sci.* **2021**, *427*, 110–117. [CrossRef]
76. Huang, C.; Liu, H.; Shi, X.; Chen, X.; Xiao, M.; Wang, Z.; Cao, J. Bifurcations in a fractional-order neural network with multiple leakage delays. *Neural Netw.* **2020**, *131*, 115–126. [CrossRef]
77. Xu, C.; Liu, Z.; Yao, L.; Aouiti, C. Further exploration on bifurcation of fractional-order six-neuron bi-directional associative memory neural networks with multi-delays. *Appl. Math. Comput.* **2021**, *410*, 126458. [CrossRef]